# High-Efficiency SOI Fiber-to-Chip Grating Couplers and Low-Loss Waveguides for the Short-Wave Infrared

Nannicha Hattasan, Bart Kuyken, Francois Leo, Eva M. P. Ryckeboer, Diedrik Vermeulen, and Gunther Roelkens

*Abstract*—We report on high-efficiency silicon-on-insulator (SOI) grating couplers and low-loss single-mode optical waveguides operating in a short-wave infrared. A −3.8 dB coupling efficiency from a standard single-mode fiber to an SOI waveguide at 2.1 $\mu$m is obtained experimentally. Single-mode waveguide losses in the short-wave infrared below 0.6 dB/cm are reported.

*Index Terms*—Grating coupler, short-wave infrared (SWIR), silicon-on-insulator (SOI) waveguide.

## I. INTRODUCTION

WHILE originally conceived for telecommunication and data communication, silicon photonics is emerging as a potential integration platform for applications covering a broader wavelength range. Particularly for spectroscopic sensing applications and nonlinear optics on the silicon platform, moving towards the short-wave infrared ($>2$ $\mu$m) is attractive. For spectroscopic sensing systems this is driven by the fact that the characteristic absorption lines of molecules of interest become much stronger at longer wavelengths, thereby increasing the sensitivity of the sensing system and lowering the footprint of the devices [1]. For nonlinear optics applications on the silicon platform, moving to longer wavelengths is driven by the absence of parasitic two-photon absorption above 2.2 $\mu$m, given the 1.12 eV band gap of silicon [2]. For both applications there is a need to develop photonic integrated components for the short-wave infrared. While several state-of-the-art silicon-based passive components at telecommunication wavelengths have been reported in the past few years [3], [4], only very few have been studied in the short-wave (SWIR) and mid-infrared (MWIR) [5], [6]. We have reported preliminary results of high-efficiency fiber-to-chip grating couplers with air cladding for the short-wave infrared in [7]. In this letter we elaborate on the design, fabrication and the comprehensive study of grating coupler characteristics over a broad parameter range, leading

to an improved coupling efficiency of −3.8 dB. We also report on the demonstration of single mode waveguides for the short-wave infrared with losses below 0.6 dB/cm. A low fiber-to-chip coupling loss and low waveguide loss are two very important prerequisites to achieve a high-performance SWIR platform.

## II. GRATING COUPLER: DESIGN AND SIMULATION

The grating coupler structure design consists of a 220 nm thick crystalline silicon layer as a waveguide layer with a 160 nm poly-silicon overlay on top of the waveguide. A 2 $\mu$m buried oxide layer is used. A polished $SiO_2$ top-cladding (1.0 $\mu$m thick) is applied and the total etch depth is fixed to 240 nm in order to be compatible with the CMOS fabrication process used to fabricate these devices. Fig. 1 represents the schematic of the grating coupler structure. The coupling efficiency to single mode fiber was assessed by evaluating the overlap integral as in equation 1

$$\eta = \left| \int E_z H_{fib,x} dx \right|^2 \tag{1}$$

where $E_z$ is the diffracted electrical field from the grating towards the superstrate, when the TE waveguide mode is launched, and $H_{fib,x}$ is the fiber mode magnetic field distribution, which is assumed to be Gaussian. The integration is carried out along a horizontal line in the superstrate.

Simulations are carried out using 2D Finite-Difference-Time-Domain (FDTD) software. The 3D nature of the problem is taken into account by analytically calculating the lateral overlap integral between the Gaussian fiber mode and the cosine-shaped silicon waveguide mode. The fiber is positioned at the optimum position along the x-direction. A 10° tilt from vertical is presumed to avoid substantial second order Bragg reflection back into the waveguide when coupling to the optical fiber. 20 grating periods are used for the simulation. The optical mode in the standard single mode fiber (SMF-28) with a core of 9 $\mu$m diameter is approximated by a Gaussian beam with a mode field diameter (MFD) of 13.3, 13.9 and 14.5 $\mu$m at 2.1, 2.2, and 2.3 $\mu$m respectively as calculated by a fully-vectorial finite element method. Fig. 2(a) illustrates the simulated fiber-to-chip coupling efficiency as a function of wavelength for 4 different grating periods (0.98 $\mu$m, 1 $\mu$m, 1.02 $\mu$m, 1.04 $\mu$m) with a 0.25 fill factor, defined as the silicon tooth width to period ratio. The gratings are etched 80 nm into the crystalline silicon waveguide layer (240 nm overall
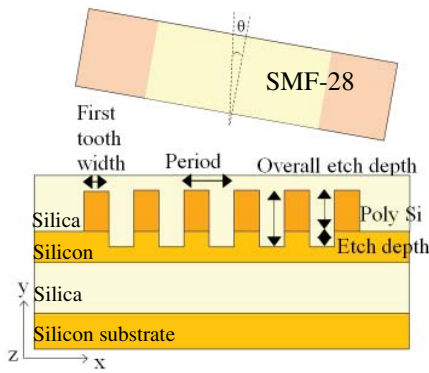
Fig. 1.   Schematic of the short-wave infrared fiber-to-chip grating coupler structure.
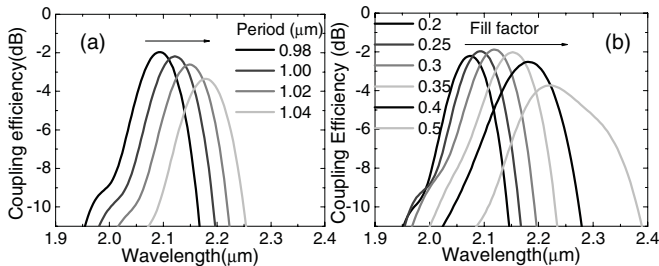


Fig. 2.   Simulated coupling efficiency for different grating parameters. (a) Coupling efficiency as a function of the grating period with fill factor 0.25. (b) Simulated coupling efficiency as a function of the fill factor (0.98 $\mu$m period, 80 nm etch depth).



Fig. 3.   (a) Simulated coupling efficiency with different grating etch depths into the crystalline silicon layer (period = 0.98 $\mu$m and fill factor = 0.25). (b) Coupling efficiency reduction due to the lateral mode mismatch between the silicon waveguide mode and the fiber mode for various wavelengths as a function of silicon waveguide width (period = 0.98 $\mu$m; fill factor = 0.25; and etch depth 240 nm).

etch depth). It can be seen that, by increasing the period, the center of the coupling spectrum shifts to longer wavelengths, in accordance with the Bragg condition. However, the coupling efficiency decreases due to the increased mode mismatch between grating coupler and fiber. In Fig. 2(b), a period of 0.98 $\mu$m and 80 nm etch depth into the crystalline silicon layer are selected and the fill factor of the grating is varied. The optimum fill factor is found to be at 0.3. By increasing the fill factor to above 0.4, the efficiency decreases substantially. Another parameter that affects the grating coupler performance is the grating-etch depth. In Fig. 3(a), a peak wavelength shift can be observed with varying etching depth in the crystalline silicon layer; however the coupling efficiency decreases slowly when the etch depth is shallower than 80 nm.

In practice, due to the fabrication process, the etch depth in the crystalline waveguide layer was fixed to 80 nm. As mentioned earlier, the MFD of a standard single mode fiber increases significantly with an increasing operation wavelength. Therefore, broader waveguides are required when operating further into the short-wave infrared, as illustrated in Fig. 3(b), where the overlap integral of the transversal mode profile in the silicon waveguide (cosine-shaped) and the Gaussian profile of the fiber mode is plotted. According to the study in [8], the width of the first tooth of the grating plays an important role in the attainable coupling efficiency. It is necessary to keep its size smaller than the subsequent teeth (300 nm) in order to achieve high coupling efficiency.

## III.   FABRICATION

The fabrication of these grating couplers was done at *imec* with 193 nm DUV lithography and dry etching in a 200 mm
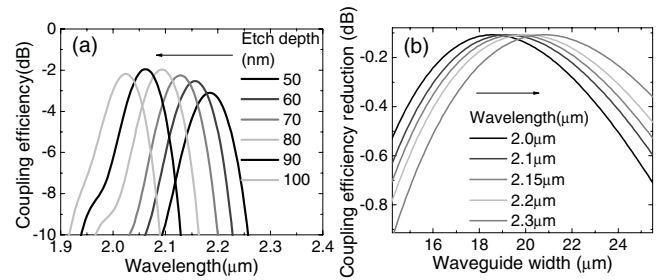
pilot line, through the multi-project wafer service ePIXfab [9]. The base wafer consists of a 220 nm crystalline silicon layer on top of 2 $\mu$m buried oxide on a silicon substrate. A 10 nm thick oxide layer is deposited, after which 160 nm poly-silicon is deposited on top of the crystalline silicon. The oxide layer is used as an etch stop layer to accurately define the 220 nm thick crystalline waveguides. The thin oxide layer does not influence the performance of the grating coupler when the TE optical mode is launched in the silicon waveguide. The grating 240 nm deep slits are formed by an ICP etching process (chlorine/fluorine-based and bromine-based chemistry). After etching the grating slits, the poly-silicon is removed, except in the grating area, by ICP etching, using the oxide layer as an etch stop. After grating structure is formed, silicon dioxide is deposited as top cladding. A photoresist mask was used for all processing steps. A scanning-electron-microscope image of such grating coupler after removing top oxide cladding is shown in Fig. 4. Fig. 4(a) represents a top-view image of the fabricated devices. The cross-section of such a grating, indicating a fill-factor of 0.3, a grating period of 1.0 $\mu$m and a grating etch depth of 239 nm, and a first tooth width of 175 nm is shown in Fig. 4(b). In this experiment, a 12 $\mu$m wide waveguide was used.

## IV.   GRATING COUPLER: EXPERIMENTAL RESULTS

The setup to characterize the grating coupler structures consists of a continuous-wave mid-infrared tunable laser (IPG Cr:ZnSe tunable laser) operating below its threshold. The generated amplified spontaneous emission is coupled to SMF-28, after which it passes a polarization controller, and is injected in the fundamental TE mode of the silicon waveguide circuit. The light is then collected by an identical grating coupler/SMF-28 combination and is coupled to a short-wave infrared optical spectrum analyzer (Yokogawa AQ6375). Fig. 5(a) shows the coupling efficiency of the grating couplers as a function of wavelength for different grating periods. The grating coupler with a period of 0.98 $\mu$m and a fill factor of 0.3 shows $-3.8$ dB coupling efficiency at a peak wavelength of 2.1 $\mu$m with a 3 dB bandwidth of 90 nm. The fringes that can be observed are Fabry–Perot interference fringes, resulting from parasitic reflections from the grating couplers. From the fringe depth the parasitic reflection from the grating couplers can be assessed.
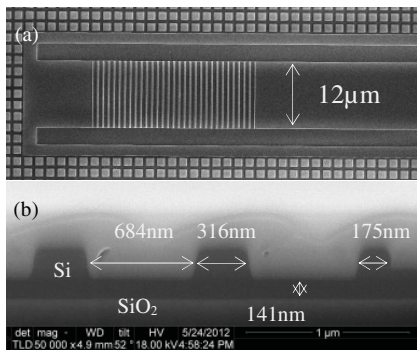
Fig. 4. Scanning electron microscope image of the fabricated short-wave infrared fiber-to-chip grating couplers. (a) Top view and (b) cross-section.
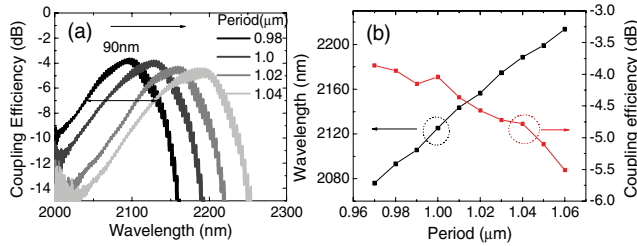


Fig. 5. (a) Coupling efficiency as a function of wavelength for different grating periods (fill factor ∼0.3). (b) Peak wavelength and coupling efficiency as a function of the grating period.

As can be seen in Fig. 5(a) the fringe depth varies from 0.5 dB at shorter wavelengths to 1.5 dB at longer wavelengths, resulting in a reflection ranging from 2.8% at shorter wavelengths to 8.5% at longer wavelengths. This is consistent with the fact that for longer wavelengths the outcoupling is closer to the surface normal and hence stronger second order Bragg reflection can be expected. Fig. 5(b) summarizes the experimentally measured increase of peak wavelength and the decrease of coupling efficiency as a function of the grating period, for a fixed fill factor of 0.3. The decrease in efficiency when going to longer wavelengths is attributed to (a) the increase of the loss in SMF at longer wavelength (i.e. the fiber loss increased from 0.008 dB/m at 2 $\mu$m to 2.3 dB/m at 2.5 $\mu$m), which cannot be completely calibrated out in the measurement system and (b) the increasing mode mismatch between the silicon waveguide mode and that of the single mode fiber at longer wavelengths.

As predicted from the simulation, the fiber-to-chip coupling efficiency can be improved by increasing the silicon waveguide width to an optimum value. In Fig. 6(a), the normalized coupling efficiency of a grating coupler with a 1.05 $\mu$m period (2225 nm peak coupling wavelength) is plotted as a function of waveguide width. An optimum coupling efficiency is obtained for a waveguide width of 20 $\mu$m. Fig. 6(b) shows the corresponding normalized coupling spectra.

## V. WAVEGUIDE LOSSES

Besides high-efficiency optical coupling between a single mode fiber and a silicon waveguide circuit, also low-loss waveguides are of paramount importance for an integration platform for short-wave infrared applications. The waveguides considered in this work are 900 nm wide and etched 220 nm deep into the 220 nm crystalline silicon guiding layer.
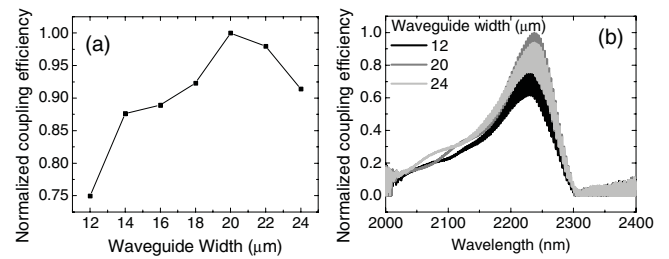


Fig. 6. (a) Normalized coupling efficiency as a function of waveguide width. (b) Corresponding normalized coupling spectra.
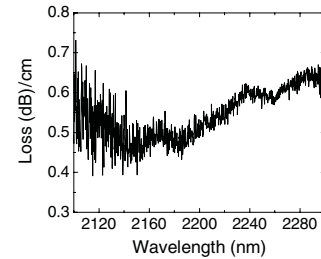


Fig. 7. Silicon-on-insulator single mode waveguide losses (220 nm by 900 nm waveguides) in the short-wave infrared.

There is no poly-silicon on top of the waveguides. The waveguide loss was assessed by cut-back measurements on 1 cm, 2 cm, 4 cm and 7 cm long waveguides. The resulting propagation loss is plotted in fig. 7, showing losses lower than 0.6 dB/cm in the short-wave infrared. These low losses are of paramount importance both in spectroscopic applications and in nonlinear optics applications, since it enhances the effective interaction length in both cases.

## VI. CONCLUSION

In conclusion, we report on the design and experimental realization of highly efficient raised fiber-to-chip grating couplers and low-loss waveguides on SOI for short-wave infrared applications. The results are showing the potential of the silicon-on-insulator waveguide platform for spectroscopic sensing applications and integrated nonlinear optics in the short-wave infrared.

## REFERENCES

[1] M. Ortsiefer, *et al.*, "Long-wavelength VCSELs for sensing applications," *Proc. SPIE*, vol. 8276, pp. 82760A-1–82760A-8, Feb. 2012.

[2] A. D. Bristow, N. Rotenberg, and H. M. van Driel, "Two-photon absorption and Kerr coefficients of silicon for 850–2200 nm," *Appl. Phys. Lett.*, vol. 90, no. 19, pp. 191104-1–191104-3, 2007.

[3] W. Bogaerts, *et al.*, "Silicon microring resonators," *Lasers Photon*, vol. 6, no. 1, pp. 47–73, 2012.

[4] P. Cheben, D.-X. Xu, S. Janz, and A. Densmore, "Subwavelength waveguide grating for mode conversion and light coupling in integrated optics," *Opt. Express*, vol. 14, no. 14, pp. 4695–4702, 2006.

[5] Z. Cheng, X. Chen, C. Y. Wong, K. Xu, C. K. Y. Fung, Y. M. Chen, and H. K. Tsang, "Focusing subwavelength grating coupler for mid-infrared suspended membrane waveguide," *Opt. Lett.*, vol. 37, no. 7, pp. 1217–1219, 2012.

[6] Z. Cheng, *et al.*, "Mid-infrared grating couplers for silicon-on-sapphire waveguides," *IEEE Photon. J.*, vol. 4, no. 1, pp. 104–112, Feb. 2012.

[7] B. Kuyken, *et al.*, "Highly efficient broadband silicon-on-insulator grating couplers for the shortwave infrared wavelength range," in *Proc. Integr. Photon. Res. Silicon Nanophoton.*, 2011, pp. 1–3, paper IMB6.

[8] G. Roelkens, D. Van Thourhout, and R. Baets, "High efficiency silicon-on-insulator grating coupler based on a poly-silicon overlay," *Opt. Express*, vol. 14, no. 24, pp. 116622–11630, 2006.

[9] *The Silicon Photonics Platform-ePIXfab*. (2012) [Online]. Available: http://www.epixfab.eu